Research on Chemical Intermediates
https://doi.org/10.1007/s11164-019-03961-7

In situ DRIFTS investigation on CeO_2/TiO_2–ZrO_2–SO_4^{2-} catalyst for NH_3–SCR: the influence of surface acidity and reducibility

Qiulin Zhang[1] · Lanying Wang[1] · Ping Ning[1] · Zhongxian Song[2] · Jie Fan[1] · Huimin Wang[1] · Tong Tang[1] · Jia Hu[1]

Received: 29 April 2019 / Accepted: 29 August 2019

Abstract

A series of CeO_2-modified TiO_2–ZrO_2–SO_4^{2-} catalysts were employed to the selective catalytic reduction (SCR) of NO_x by NH_3. The obtained results indicated that the interaction between CeO_2 and TiO_2–ZrO_2–SO_4^{2-} contributed to the increased reducibility and decreased surface acidity with the augment of CeO_2. The in situ DRIFTS results suggested that suitable surface acidity and reducibility could be offered by increasing the ceria loadings from 24 to 40 wt%. The amount of adsorbed NH_3 species, amide species ($–NH_2$) and activated nitrate was increased with the augment of ceria. Excessive addition of CeO_2 (80 wt%) resulted in the lacking of surface acid sites and induced the inert nitrate species generation on the catalysts surface.

Keywords NO_x · NH_3–SCR · CeO_2 · TiO_2–ZrO_2–SO_4^{2-} · Surface acidity · DRIFTS

Introduction

Nitrogen oxides (NO_x), rooted in automotive exhausts and stationary sources, are one of the atmospheric pollutants resulting in some environmental problems and threat to health [1–3]. Selective catalytic reduction of NO_x by ammonia (NH_3–SCR) is known as the state-of-the-art method for eliminating NO_x [4]. The vanadium-based

Electronic supplementary material The online version of this article (https://doi.org/10.1007/s11164-019-03961-7) contains supplementary material, which is available to authorized users.

✉ Ping Ning
ningping_58@126.com

[1] Faculty of Environmental Science and Engineering, Kunming University of Science and Technology, Kunming 650500, People's Republic of China

[2] Henan Province Key Laboratory of Water Pollution Control and Rehabilitation Technology, Henan University of Urban Construction, Pingdingshan 467000, People's Republic of China

Published online: 10 September 2019

catalysts have been commercially practiced for decades to cut down the emission of NO_x [5]. However, there are some obvious drawbacks of vanadium-based catalysts, for instance, the confined temperature window, the virulence of vanadium species and low N_2 selectivity [6, 7]. To avoid these problems mentioned above, more and more researchers are aimed to develop eco-friendly catalysts with excellent NO_x conversion and N_2 selectivity.

Recently, the ceria-based catalysts have attracted great interest as SCR catalysts on account of its nontoxicity, favorable reducibility and brilliant oxygen storage capability (OSC) [8–11]. The oxygen vacancy resulting from redox cycling between Ce^{3+} and Ce^{4+} is conducive to the adsorption and activation of NO [12]. Meanwhile, it is widely reported that surface acid plays a vital role in NH_3–SCR reaction [13, 14]. A suitable surface acid for SCR catalyst can facilitate the adsorption of ammonia and prevent ammonia oxidation in the elevated temperature, obtaining meliorative catalytic activity [15, 16]. A series of acid-modified CeO_2 catalysts have been synthesized, such as CeO_2–PO_4^{3-} [17–19], CeO_2–SO_4^{2-} [12, 20], and CeO_2 modified by solid acid [21–25]. Among them, ceria-based catalysts modified by solid acid exhibit efficient denitration and high N_2 selectivity owing to the enrichment of surface acidity. Yu et al. [16] and Liu et al. [26] proved that surface acid sites were notably increased due to the introduction of ceria to solid acid, and the SCR activity was then markedly enhanced for the facilitating adsorption and activation of ammonia. We also developed several novel catalysts [27–30], a series of ceria-based catalysts modified by phosphotungstic acid, silicotungstic acid and zirconium phosphate were prepared and studied. In our previous work [31], we synthesized a novel CeO_2/TiO_2–ZrO_2–SO_4^{2-} catalysts with excellent NO_x conversion in a wide temperature range. We found that the introduction of Ce could markedly increase the surface acidity. Moreover, we studied the reaction mechanism on the CeO_2/TiO_2–ZrO_2–SO_4^{2-} catalysts via in situ DRIFTS. However, it was still unclear that the effect of CeO_2 loadings on reducibility, surface acidity and reaction pathway over CeO_2/TiO_2–ZrO_2–SO_4^{2-} catalysts. To further investigate the effect of reducibility and surface acidity on NH_3–SCR activity, the work of this paper was carried out.

It was found that the surface acidity and reducibility were important for SCR reaction. However, it was still not clear about the effect of the variational reducibility and surface acid on the SCR reaction of solid acid-modified ceria-based catalysts.

In this work, a variety of ceria-based catalysts with various surface acidity and reducibility were prepared via supporting different amounts of CeO_2 on the solid superacid TiO_2–ZrO_2–SO_4^{2-}. We attempt to detailedly reveal the effects of surface acidity and reducibility on NH_3–SCR reaction were investigated by H_2-TPR and in situ DRIFTS.

Experimental

Synthesis of materials

The TiO_2–ZrO_2 (Ti: Zr = 1, mass ratio) was synthesized by coprecipitation method. 6.96 g zirconium nitrate and 6.46 g titanyl sulfate were dissolved in 60 mL distilled

water, respectively. 0.8 g polyethylene glycol 4000 was added after the two solutions mixed together. $NH_3{\cdot}H_2O$-$(NH_4)_2CO_3$ buffer solution was added into the above aqueous solution dropwise by vigorously stirring till the pH reached 9–10. The precipitate was aged at 80 °C for 3 h in the mother liquid, followed by filtering and washing with distilled water, the precipitate was dried. Then, the prepared TiO_2–ZrO_2 powder was immersed to 0.5 M H_2SO_4 solution for 3 h following by filtration. The 2 g TiO_2–ZrO_2 powder was immersed in 0.5 M H_2SO_4 solution for 3 h, and then sulfated TiO_2–ZrO_2 was filtered and washed with distilled water. Finally, the sulfated TiO_2–ZrO_2 cake was dried and calcined at 550 °C for 3 h. The obtained solid superacid support TiO_2–ZrO_2–SO_4^{2-} sample was signed as TZS.

Preparation of catalysts

The CeO_2/TiO_2–ZrO_2–SO_4^{2-} catalysts at various CeO_2 loadings for 4, 12, 24, 40, 60 and 80 wt% were synthesized by wetness impregnation method. The cerium nitrate was regarded as the precursor CeO_2. Calculated TiO_2–ZrO_2–SO_4^{2-} powder was dissolved into the precursor solution and stirred at 60 °C for 5 h, followed by the samples dried overnight. Finally, the powder was calcined at 550 °C for 3 h. The obtained catalysts were named as xCe/TZS ($x = 4$, 12, 24, 40, 60 and 80).

Activity measurements

The performance tests were conducted in a fixed-bed quartz reactor. The reactant gas was as follows: 600 ppm NH_3, 600 ppm NO, and 5 vol% O_2, balanced by N_2. The total flow rate of gas mixture was 400 mL/min at a GHSV of 48,000 h^{-1}. The effluent gas of NO and NO_2 was detected with a flue gas analyzer (ECOM J2KN). The production of N_2O was measured by GC (Fuli, 9790, China). The NH_3–SCR activity was determined by NO_x conversion:

$$NO_x \text{ conversion} = \frac{[NO_x]_{in} - [NO_x]_{out}}{[NO_x]_{in}} \times 100\%$$

where $[NO_x]_{in}$ and $[NO_x]_{out}$ represented the inlet and outlet concentration of NO_x, respectively.

Characterization of catalysts

H_2-TPR was carried out in a quartz reactor with a TCD. 30 mg catalysts were treated for 1 h at 400 °C under N_2 atmosphere (30 mL/min). When the temperature cooled down to 30 °C, the introduce gas was switched to 5%H_2/Ar. The reactor temperature was range from 30 to 900 °C.

NO-TPD was conducted in a fixed-bed quartz reactor using 50 mg catalyst. The sample was purged under 499 ppm NO at room temperature after being pretreated in N_2 at 400 °C for 30 min. The temperature was raised to 600 °C at a rate of 8 °C/min.

NH_3-TPD was carried out with a quadrupole mass spectrometer (PREVAC) with 50 mg sample. Prior to each experiment, the sample was pretreated in pure N_2 at

400 °C for 30 min. Then, the sample was saturated with 4000 NH_3/Ar at a flow rate of 300 mL/min for 2 h. Desorption was performed by heating the sample in pure Ar from 50 to 600 °C with a rate of 8 °C/min.

In situ DRIFT spectra were obtained at Nicolet iS50 FTIR spectrometer. The sample was pre-treated in 5 vol% O_2/N_2 at 400 °C for 30 min (100 mL/min) before collecting background. For the NH_3 adsorption at various temperatures, 600 ppm NH_3 in N_2 was introduced on the catalysts for 30 min and then switched to N_2 at appointed temperature. As for the transient studies, 600 ppm NH_3 (or 600 ppm $NO + O_2$) was injected in the pre-adsorbed NO_x (or NH_3 species) samples at 225 and 500 °C. For the $NH_3 + NO + O_2$ co-adsorption at 225 and 500 °C, the reactant gas was introduced to samples for 30 min.

Results

SCR activities

The NO_x conversion of *x*Ce/TZS catalysts is presented in Fig. 1. As illustrated in Fig. 1a, the low-temperature NH_3–SCR performance was significantly enhanced by increasing the CeO_2 loadings from 4 to 40%, and more than 90% NO_x conversion achieved over 40Ce/TZS sample between 225 and 475 °C. However, excessively high content of CeO_2 (80 wt%) was incapable to further improve the low-temperature catalytic performance but to narrow the temperature window of *x*Ce/TZS samples. Particularly for the 80Ce/TZS catalyst, the complete conversion of NO_x began to decrease at 300 °C and sharply dropped to 20% at 500 °C. Based on the previous studies [17, 20, 31], although pure CeO_2 possessed excellent reducibility, the excessive surface active oxygen resulted in ammonia oxidation reaction at elevated temperature on catalysts. Thus, this phenomenon usually caused the decline of N_2 selectivity and activity at high temperature. Even though the generation of N_2O was enhanced obviously with the increase in ceria, it was less than 20 ppm in whole temperature. It could be found that *x*Ce/TZS catalysts exhibited excellent N_2 selectivity.

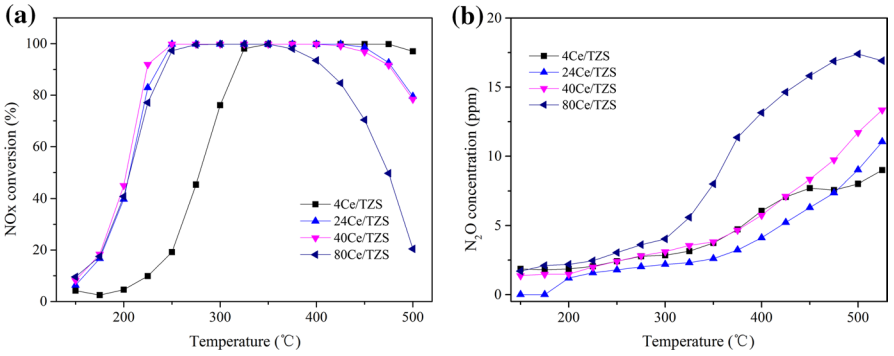

Fig. 1 NH_3–SCR performance of the catalysts: **a** NO_x conversion and **b** N_2O concentration. Reaction conditions: 600 ppm NO, 600 ppm NH_3, 5 vol% O_2, balance N_2, GHSV = 48,000 h^{-1}

As described in Fig. 1b, at elevated temperature, the generation of N_2O was enhanced obviously with the increase in ceria, but it was less than 20 ppm in whole temperature, suggesting that *x*Ce/TZS catalysts owned excellent N_2 selectivity. Therefore, the sharply decreasing activity could be attributed to the ammonia oxidation reaction. Obviously, it was important for NH_3–SCR reaction to possess appropriate reducibility.

Surface redox ability

Figure 2a describes the H_2-TPR curves of Ce/TZ catalysts. Two H_2 consumption peaks were observed over 4Ce/TZS catalyst, while only one peak was noticed on 24 Ce/TZS, 40 Ce/TZS and 80Ce/TZS catalysts. It was reported that the peaks around 582 °C were assigned to the sulfate anions infirmly boned to the surface [32], and the peaks at 640 °C were attributed to the sulfate species strongly linked with the surface species [33]. Gannoun and co-workers [12, 34] reported that peaks at 646 and 560 °C were assigned to the reduction of bulk cerium sulfates and surface cerium sulfates, respectively. Besides, the reduction peaks at 454 °C were attributed to the reduction of surface Ce^{4+} to Ce^{3+} [35]. It was clearly seen from Fig. 2a, the reductive peaks obviously moved to lower temperature with the augment of ceria loadings, suggesting that the reducibility was significantly enhanced via increasing ceria loadings. For 24 Ce/TZS, 40Ce/TZS catalysts, the areas of H_2 consumption peaks were larger than surplus catalysts, illustrating that the two catalysts possessed excellent reducibility resulting in outstanding SCR activity. Meanwhile, 24Ce/TZS, 40Ce/TZS catalysts had similar type of reduction peak and operation window. However, the two catalysts had alike NO_x conversion within 225–475 °C, but 24Ce/TZS owned better N_2 selectivity than 40Ce/TZS catalysts (as shown in Fig. 1b). The NO_2 concentration of catalysts at 200 °C is described in Fig. 2b. At low temperature, the NO_2 concentration was obviously enhanced with the increase in CeO_2 loadings. Combined with the consequence of NH_3–SCR performance and H_2-TPR, it could be

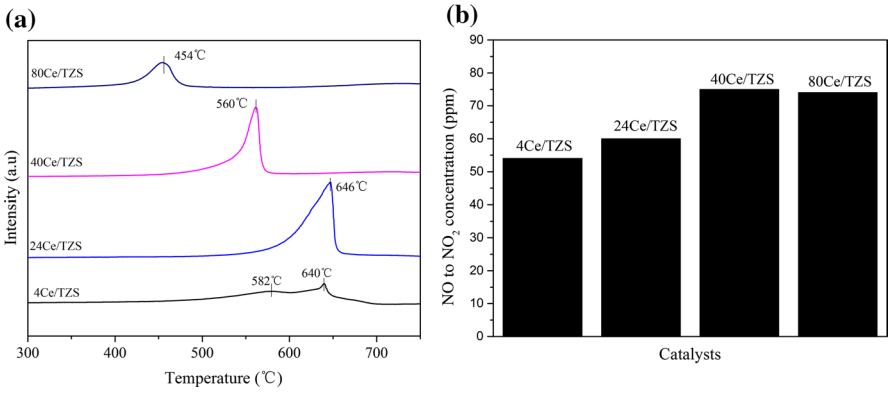

Fig. 2 H_2-TPR curves (**a**) and NO_2 concentration at 200 °C (**b**) of different catalysts. Reaction conditions: 600 ppm NO, 5 vol% O_2, balance N_2, GHSV = 48,000 h^{-1}

concluded that the optimal ceria loadings lead to appropriate reducibility and surface acidity, and then lead to the best NH_3–SCR activity.

TPD profiles

In order to reveal the variation and type of the surface acid sites on the *x*Ce/TZS catalysts, NH_3-TPD test was carried out. As previous reports [36], the desorption peaks at 100–250 °C were assigned to the weak acidity, and the desorption peaks at 250–500 °C were attributed to the strong acidity. As shown in Fig. 3a, the NH_3 desorption peaks on the *x*Ce/TZS catalysts appeared at 100–200 °C, this indicated that weak acidity occurred on the *x*Ce/TZS catalysts. Moreover, with the increase in CeO_2 loadings, the quantity of surface acidity was distinctly decreased. This phenomenon indicated that excess CeO_2 might cover the acid sites on the catalysts leading to the decline of surface acidity.

In order to investigate the effect of CeO_2 on NO adsorption/desorption behaviors, NO-TPD experiments are conducted and shown in Fig. 3b. All of the catalysts exhibited desorption peaks at above 100 °C attributing to desorption of chemisorbed NO_x species [11]. Moreover, the first peak was at 150 °C and the second one was around 280 °C on the 4Ce/TZS catalyst. For other catalysts, the peaks were shifted to lower temperature, and the intensity was weakened. It was accounted for the adsorbed NO_x species were stable over the 4Ce/TZS catalyst. However, this was not conducive to the NH_3–SCR performance.

In situ DRIFTS results on *x*Ce/TZS catalysts

The DRIFTS of NH_3 adsorption/desorption

To investigate the types, the intensity of surface acid and the stability of ad-NH_3 species over *x*Ce/TZS catalysts, the DRIFTS of NH_3 adsorption/desorption upon

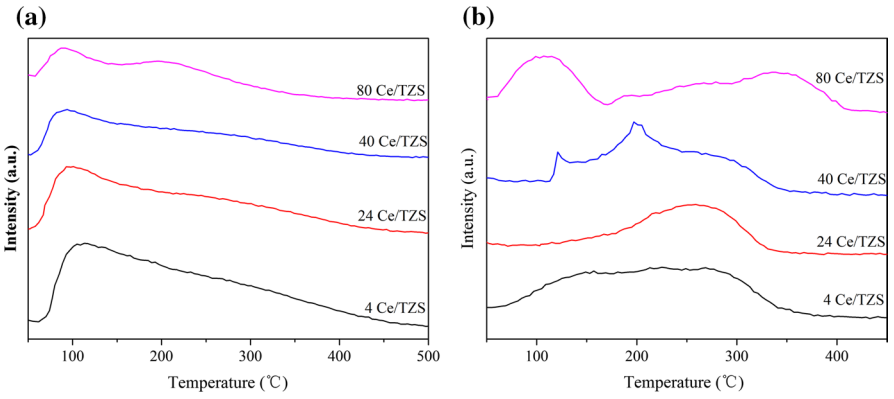

Fig. 3 TPD profiles over *x*Ce/TZ catalysts: **a** NH_3-TPD; **b** NO-TPD

various temperatures were tested. As described in Fig. 4, the peaks around 1280 and 1600 cm^{-1} were assigned to the coordinated NH_3 species linked to Lewis acid sites [37, 38], respectively. The peaks around 1430 and 1680 cm^{-1} were assigned to the NH_4^+ ions bonded to Brønsted acid sites. [39, 40]. It could be clearly seen from Fig. 4, although Lewis and Brønsted acid sites were existed on *x*Ce/TZS catalysts, the intensity of them was different. At low temperature, the intensity of NH_4^+ ions was stronger than coordinated NH_3 species, but declined sharply when the temperature rose. It suggested that the coordinated NH_3 species were more stable than NH_4^+ ions. The strength of surface acid was strong on the 4Ce/TZS and 40Ce/TZS, while it was weak on the 24Ce/TZS and 80Ce/TZS. Peng et al. [21] proved that criea could offer Lewis acid sites, but the surface acidity sharply decreased with excessive criea loadings. Combined with the consequence of NO_x conversion, the shortage of surface acidity resulted in inferior activity at elevated temperature. Furthermore, with the elevation of the reaction temperature, the peak attributed to NH_4^+ species (1680 cm^{-1}) declined more observably than that of the bands ascribed to coordinated NH_3. Moreover, the bands assigned to both Brønsted and Lewis acid sites were vanished under 450 °C on 80Ce/TZS. It was implied that a lack of ad-NH_3 species at elevated temperature.

NH_3 adsorption

In situ DRIFTS spectra of the surface absorbed NH_3 species at specific temperature were recorded. The ad-NH_3 species of *x*Ce/TZS catalysts at low temperature are illustrated in Fig. 5, several same peaks of ad-NH_3 species were observed on all *x*Ce/TZS samples, including coordinated NH_3 (1600 and 1280 cm^{-1}), NH_4^+ species (1680 and 1430 cm^{-1}). Except for 4Ce/TZS catalyst, some new adsorbed species were detected over the other catalysts. The peaks centered around 1550 and 1170 cm^{-1} were attributed to intermediate from oxidation of NH_3 and coordinated NH_3 species [39, 41], respectively. Several peaks around 1510, 1330 and 1090 cm^{-1} were ascribed to amide (–NH_2) species that resulted from the deprotonation of ammonia [25, 39, 42]. It was obvious that the amount of amide species was increased with the addition of ceria. Xiong et al. [43] and Wang et al. [44] proved that amide species was a vital intermediate for E–R mechanism. Connecting with the consequences of NH_3–SCR activity and H_2-TPR, it could be concluded that the reaction was certainly promoted via increasing CeO_2 loadings. However, the emerging peak at 1550 cm^{-1} verified that exceeding reducibility can lead to ammonia oxidation, which was adverse for SCR reaction.

The ad-NH_3 species above 450 °C are recorded and presented in Fig. S1. Despite the peak centers were invariable, the intensity and amount of adsorbed species significantly reduced owing to its poor stability. The peaks at 1680 and 1280 cm^{-1} were completely disappeared on all catalysts. Besides, the peak at 1600 cm^{-1} vanished, as well as the peak around 1550 cm^{-1} on 80Ce/TZS catalyst. However, the peak ascribed to amide around 1330 cm^{-1} was observed on 4Ce/TZS catalyst, it was awfully different from the results obtained at low temperature. Associated with the activity results, the appearance of activate –NH_2 over the 4Ce/TZS certainly accelerated SCR reaction in elevated temperature range. For 24Ce/TZS and 40Ce/TZS

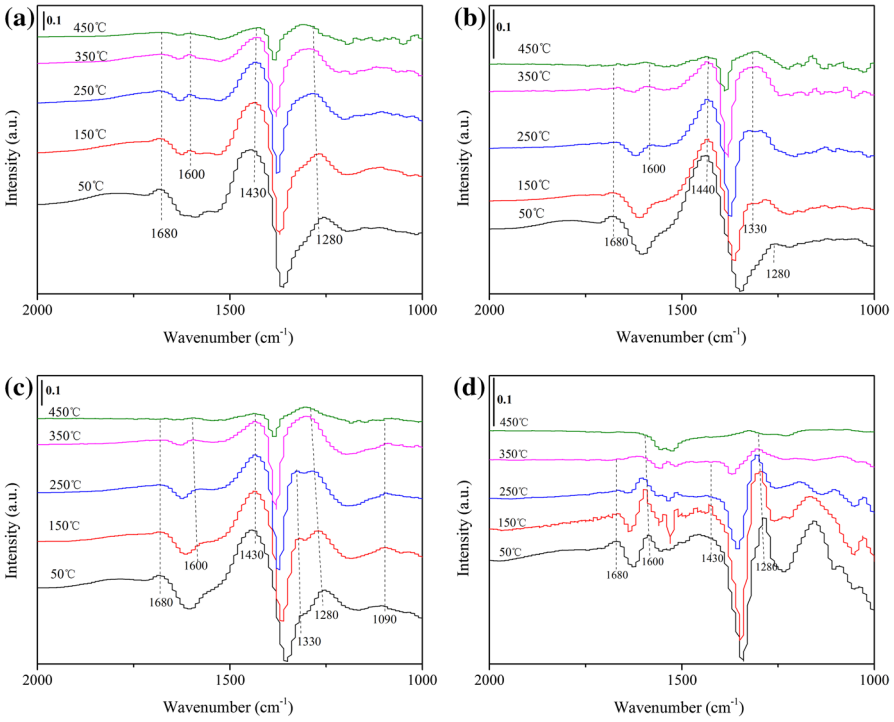

Fig. 4 NH_3-DRIFT patterns of catalysts. (**a** 4Ce/TZS, **b** 24Ce/TZS, **c** 40Ce/TZS and **d** 80Ce/TZS)

catalysts, the lack of surface acidity resulted in a slightly descending NO_x conversion. The disappeared bands around 1550 and 1600 cm^{-1} were combined with the results obtained in previous figures; it could be positively inferred that the adsorption of NH_3 occurred at reductive sites instead of acid site, which owned weak stability at elevated temperature.

$NO + O_2$ co-adsorption

The IR spectra of $NO + O_2$ adsorption on *x*Ce/TZS catalysts at certain temperature were recorded. As depicted in Fig. 6, the peaks in all DRIFT spectra were assigned to gaseous NO_2 (1620 cm^{-1}) and nitro compounds (M-NO_2, 1390 and 1360 cm^{-1}) [26, 45, 46], respectively. The emerging peak at 1570 cm^{-1} over 40Ce/TZS catalyst was corresponded to bidentate nitrate when the sample exposed to $NO + O_2$ after 5 min [3]. The another new band around 1220 cm^{-1} was assigned to bridging nitrate [47]. Evidently, more nitrate species generated on 80Ce/TZS catalyst because of the excessive reducibility [48]. The peaks centered at 1550, 1030 cm^{-1} were assigned to bidentate nitrate [17, 49]. The peaks around 1270, 1110 and 1150 cm^{-1} were attributed to monodentate and bridging nitrate, respectively [25, 50, 51]. However, according to the acquired SCR performance consequence, it could be concluded that inactive nitrate species were produced on 80Ce/TZS. Similarly, the adsorbed NO_x

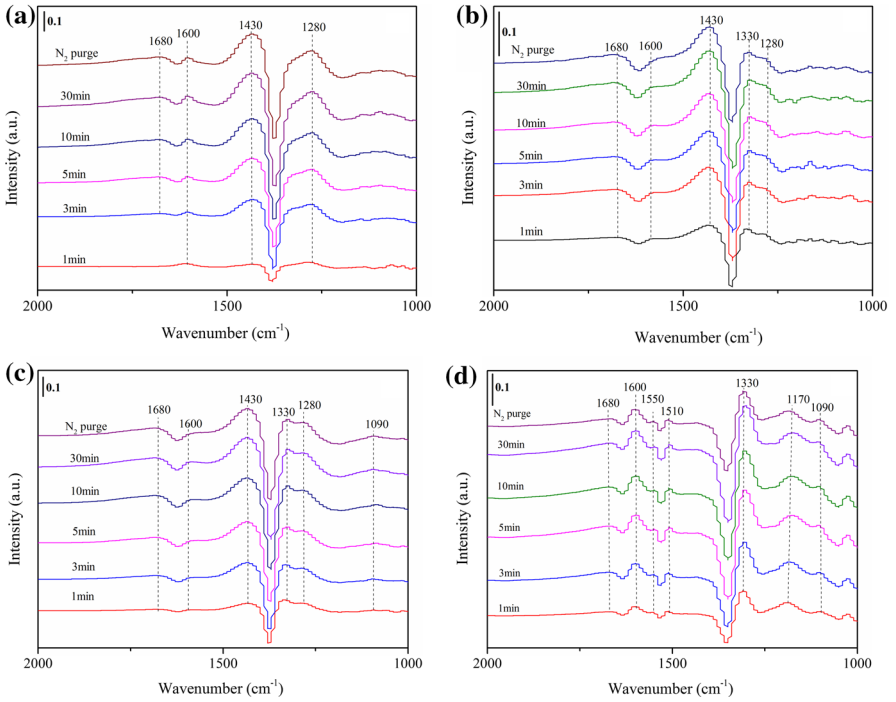

Fig. 5 DRIFTS of adsorbed species on **a** 4Ce/TZS, **b** 24Ce/TZS, **c** 40Ce/TZS and **d** 80Ce/TZS catalysts upon the passing of 600 ppm NH_3 at 225 °C

species above 450 °C were recorded. As described in Fig. S2, the adsorbed gaseous NO_2 (1620 cm^{-1}) became infirm, while the M-NO_2 compounds (1390 cm^{-1}) exhibited stronger than the spectra obtained at low temperature. Furthermore, the peak at 1570 cm^{-1} disappeared on 40Ce/TZS, while the bands around 1620, 1170 and 1030 cm^{-1} were invisible. A emerging peak was detected around 1520 cm^{-1} assigned to monodentate nitrate [52]. Different from the case of ad-NH_3 species in Figs. 6 and S1, ad-NO_x species were readily oxidized to nitrate species, which were more stable on the catalysts even after the temperature elevated to 500 °C.

Reaction between $NO + O_2$ and NH_3 ad-species

In this experiment, the *x*Ce/TZS catalysts were pre-treated with 600 ppm NH_3 and then switched to 600 ppm NO + 5 vol% O_2. The IR spectra are illustrated in Fig. 7. According to the previous reports, the ad-NH_3 species over catalysts gradually decreased upon introducing in $NO + O_2$, manifested their reduction via reacted with gaseous NO_x/surface N_xO_y species. The reaction mentioned above called E–R mechanism, which was one of the vital pathways for SCR reaction [53]. It could be clearly observed from Fig. 7a, all the ad-NH_3 species were steady on 4Ce/TZS catalyst even after switching the gas to $NO + O_2$ for 30 min. However, as depicted in Fig. 7b–d, after introducing $NO + O_2$, the intensity of

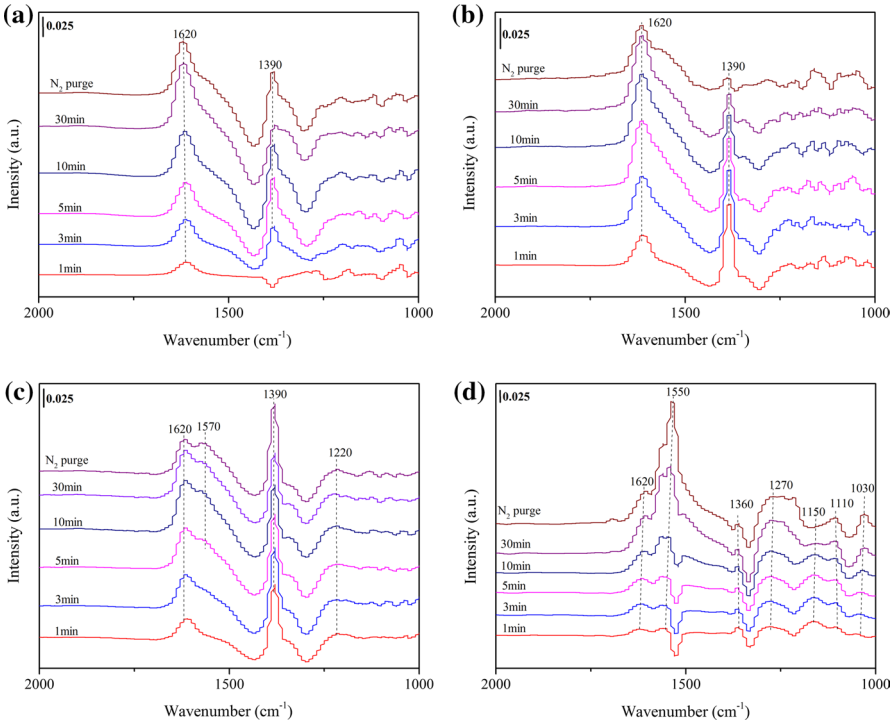

Fig. 6 DRIFTS of adsorbed species on **a** 4Ce/TZS, **b** 24Ce/TZS, **c** 40Ce/TZS and **d** 80Ce/TZS catalysts upon the passing 600 ppm NO + 5 vol% O_2 at 225 °C

ad-NH_3 species became gradually weak within 10 min. It was suggested that the reaction between gaseous NO_x and NH_3 pre-adsorbed was quite difficult at low temperature on 4Ce/TZS catalyst. Meanwhile, as exhibited in Fig. S3, once introduced the NO + O_2 gas within 1 min, the ad-NH_3 was thoroughly consumed, and then the peaks of ad-NO_x species were appeared within 3 min. Li et al. [54] reported that ammonia was firstly adsorbed over catalyst surface, followed by activated to produce –NH_2. According to Figs. 5 and S3, it could be speculated that ad-NH_3 species was consumed hard by NO_x species owing to the shortage of amide species at low temperature. Furthermore, the reaction was faster than that occurred at low temperature, it was manifested that the E–R mechanism was motivated with the elevated temperature, as reported by Zhang et al. [14] Moreover, as illustrated in Fig. 7b–d, the bands of coordinated NH_3 species (1600 and 1280 cm^{-1}) were vanished during 5 min, while the peak of NH_4^+ ion (1430 cm^{-1}) still visible within 10 min. For the reaction at elevated temperature on 24Ce/TZS, 40Ce/TZS and 80Ce/TZS catalysts, DRIFT spectra of adsorbed reactants on them are described in Fig. S3, which were mainly similar with that exhibited in Fig. 7. It seemed that coordinated NH_3 was more active than NH_4^+ ion.

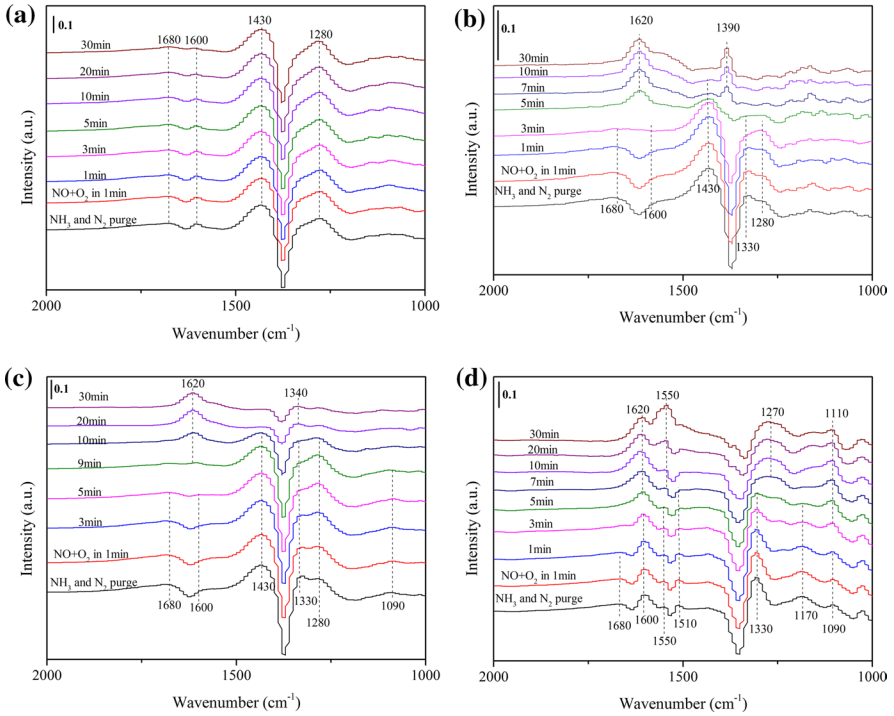

Fig. 7 DRIFT spectra obtained at 225 °C upon passing 600 ppm NO + 5 vol% O_2 over the **a** 4Ce/TZS, **b** 24Ce/TZS, **c** 40Ce/TZS and **d** 80Ce/TZS catalysts with pre-adsorbed NH_3 species

Reaction between NH_3 and NO + O_2 ad-species

The DRIFT spectra of the NO_x pre-adsorbed *x*Ce/TZS catalysts upon passing in NH_3 at 225 °C were recorded. Distinctly, it can be seen from Fig. 8 that the surface of *x*Ce/TZS catalysts was covered by homologous NO_x species presented in Fig. 7. Diverse from the situation in Fig. 7, the pre-adsorbed NO_x species were fleetly disappeared over catalysts surface after switched to NH_3 for 1 min, then the peaks of NH_3-derived species were distinctly detected within the first 3 min. This phenomenon suggested that it was easy for NH_3 to adsorb over NO_x pre-adsorbed samples. Moreover, the ad-NH_3 and ad-NO_x species was feasibly reacted due to ad-NO_x species coverage, as reported by Yang et al. [55]. Combined with the case presented in Fig. 7, it confirmed that the SCR reaction over *x*Ce/TZS followed simultaneously E–R and L–H mechanism. Besides, the generated ad-NO_x species were not exactly reactive. As illustrated in Fig. 8d, the peaks around 1550 and 1030 cm^{-1} kept inert on 80Ce/TZS catalyst after introducing NH_3 for 30 min. It has been verified that not all adsorbed NO_x species were activated on ceria-based catalysts. Yang et al. [56] discovered that bidentate nitrate was a spectator on Ce/TiO_2 catalysts. On the contrary, ad-NH_3 species were reactive with other ad-NO_x species, including gaseous NO_2 (1620 cm^{-1}), M-NO_2 (1390 cm^{-1}), monodentate (1270 cm^{-1}) and bridging nitrate (1220 cm^{-1}). The DRIFT spectra of adsorbed reactants at high temperature

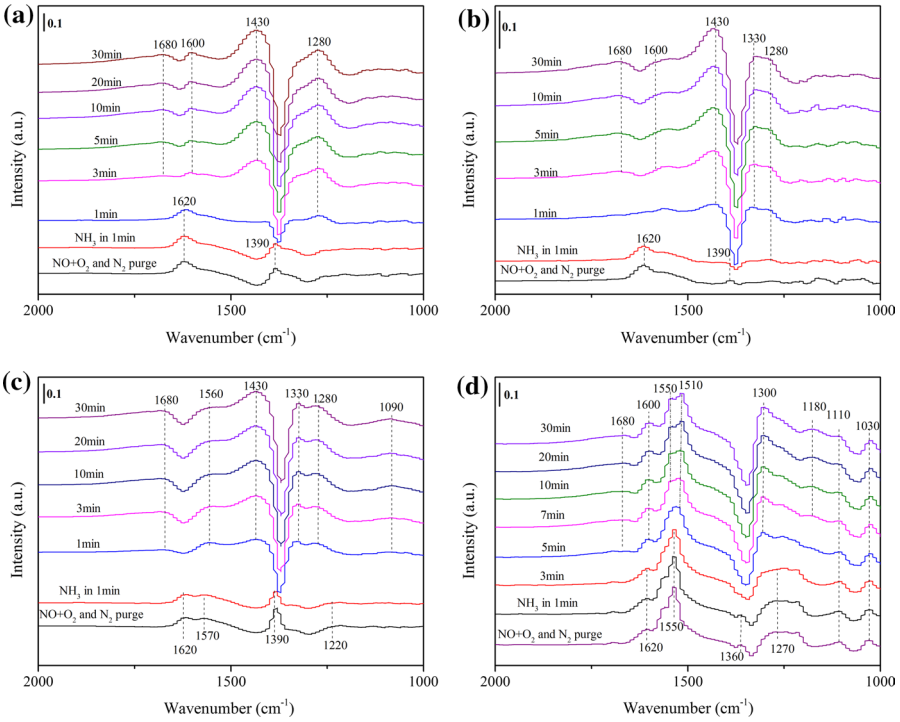

Fig. 8 DRIFT spectra obtained at 225 °C upon passing 600 ppm NH_3 over the **a** 4Ce/TZS, **b** 24Ce/TZS, **c** 40Ce/TZS and **d** 80Ce/TZS catalysts with pre-adsorbed NO + 5 vol% O_2 species

over *x*Ce/TZS samples are shown in Fig. S4. The absence of inert ad-NO_x species and the generation of vibrant nitrate accelerated the reaction.

Co-adsorption of $NO + NH_3 + O_2$

Figure 9 presents the DRIFT spectra of *x*Ce/TZS catalysts in a flow of $NH_3 + NO + O_2$ at 225 °C. The case of adsorbed species was similar to the consequences presented in Fig. 4. At low temperature (225 °C), the coordinated NH_3 (1600, 1280 and 1170 cm^{-1}), NH_4^+ ion species (1680 and 1430 cm^{-1}) and amide (1510, 1330 and 1090 cm^{-1}) were detected on *x*Ce/TZS catalysts. The intermediate (1550 cm^{-1}) were generated on 80Ce/TZS catalyst sample due to the oxidation of NH_3. However, no bands attributed to ad-NO_x species were detected. Associated with the consequences obtained in Figs. 7 and 8, it can be inferred that the reaction between ad-NH_3 species and gaseous NO_x species, as well as ad-NH_3 species and ad-NO_x species, was occurred on Ce/TZS catalysts. But the latter reaction was easier than former at low temperature. From the catalytic activity consequence achieved in Fig. 1, it was reasonable to conclude that ad-NO_x was rapidly consumed by absorbed NH_3 species via L–H mechanism. The DRIFT spectra of co-adsorption reaction at elevated temperature (500 °C) are presented in Fig. S5. Compared with the adsorption exhibited in Fig. S1, the peak around 1620 cm^{-1} might be the overlap

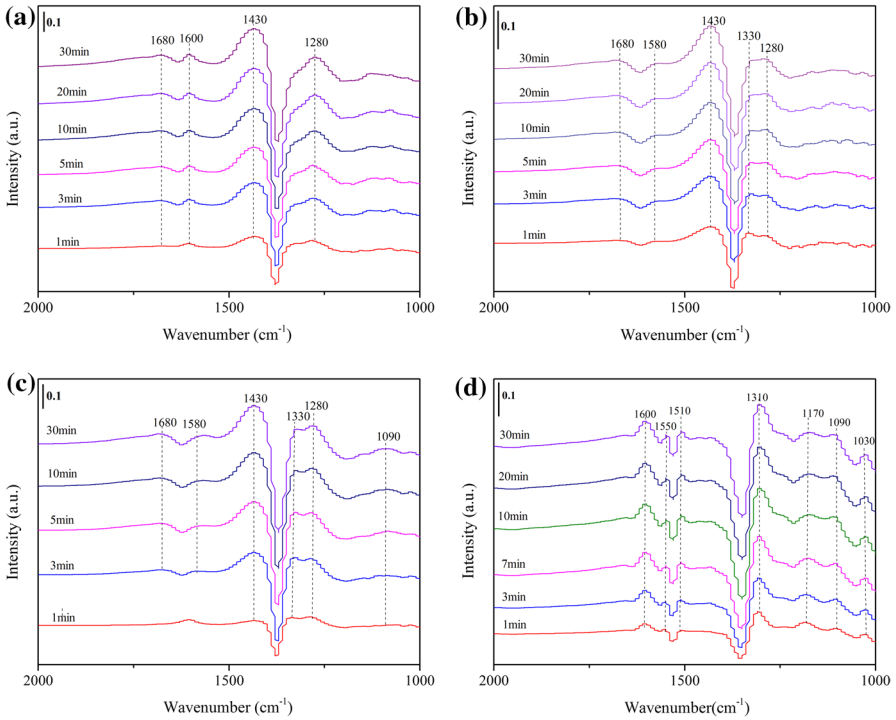

Fig. 9 DRIFT spectra of **a** 4Ce/TZS, **b** 24Ce/TZS, **c** 40Ce/TZS and **d** 80Ce/TZS catalysts in the flowing 600 ppm NH_3 + 600 ppm NO + 5 vol% O_2 at 225 °C

of gaseous NO_2 and coordinated NH_3. The band around 1430 cm^{-1} still could be observed on catalysts, suggesting that the absorbed NH_3 species on Brønsted acid sites was more stable and inert than ad-NH_3 bonded to Lewis acid sites. This consequence was in accordance with the conclusion acquired at section of *3.3.3*. Notably, the activated monodentate nitrate (1520, 1120 and 1090 cm^{-1}) and bridging nitrate (1220 cm^{-1}) were appeared on 40Ce/TZS and 80Ce/TZS catalysts. It could be deduced that ad-NH_3 species were reacted with gaseous NO_x species though E–R mechanism.

Consequently, the results above could be summarized. (1) The L–H pathway was predominant at low temperature, while the E–R pathway was leading at elevated temperature on xCe/TZS catalysts for SCR reaction. (2) The coordinated NH_3 species was more reactive than that NH_4^+ ion species. (3) The generation of inert bidentate nitrate species was increased with the augment of ceria.

Conclusion

A sequence of Ce/TZS catalysts with disparate contents of CeO_2 were synthesized and showed splendid catalytic performance within a wide reaction temperature window for NH_3–SCR reaction. With the increase in CeO_2 loadings, the reducibility

of catalyst was enhanced, owing to the the increase in surface CeO_2 species. Furthermore, the effect for reaction pathway of CeO_2 loadings was inferred via the in situ DRIFTS consequence. The amount of surface acid sites, activated adsorbed NO_x species and amide species ($–NH_2$) identified as the important intermediates increased with the addition of ceria from 4 to 40 wt%. The reaction was boosted by the increase in activated species, resulting in a excellent NO_x conversion. However, when the addition of ceria reached 80 wt%, the occurrence of ammonia oxidation due to a shortage of acidity and the generation of inert nitrate owed to the excessive reducibility contributed to the decline of NH_3–SCR performance. Therefore, it was crucial to gain a balance between reducibility and surface acidity for Ce/TZS catalysts to achieve an excellent NH_3–SCR performance.

Acknowledgements This work was supported by the National Natural Science Foundation of China (21666014).

References

1. Y. Zhao, L. Duan, T. Larssen, L.H. Hu, J.M. Hao, Environ. Sci. Technol. **41**, 1815 (2007)
2. S.P. Luo, W.T. Zhou, A.J. Xie, F.Q. Wu, C. Yao, X.Z. Li, S.X. Zuo, T.H. Liu, Chem. Eng. J. **286**, 291 (2016)
3. L.L. Li, L. Zhang, K.L. Ma, W.X. Zou, Y. Cao, Y. Xiong, C.J. Tang, L. Dong, Appl. Catal. B **207**, 366 (2017)
4. F. Nakajima, I. Hamada, Catal. Today **29**, 109 (1996)
5. Y. Jiang, X. Gao, Y.X. Zhang, W.H. Wu, H. Song, Z.Y. Luo, K.F. Cen, J. Hazard. Mater. **274**, 270 (2014)
6. S. Djerad, M. Crocoll, S. Kureti, L. Tifouti, W. Weisweiler, Catal. Today **113**, 208 (2006)
7. M. Yates, J.A. Martín, M.Á. Martín-Luengo, S. Suárez, J. Blanco, Catal. Today **107–108**, 120 (2005)
8. M.V. Ganduglia-Pirovano, A. Hofmann, J. Sauer, Surf. Sci. Rep. **62**, 219 (2007)
9. X. Gao, Y. Jiang, Y. Zhong, Z.Y. Luo, K.F. Cen, J. Hazard. Mater. **174**, 734 (2010)
10. J.X. Zhang, S.L. Zhang, W. Cai, Q. Zhong, Appl. Surf. Sci. **268**, 535 (2013)
11. L. Chen, J.H. Li, M.F. Ge, J. Phys. Chem. C **113**, 21177 (2009)
12. H.Z. Chang, L. Ma, S.J. Yang, J.H. Li, L. Chen, W. Wang, J.M. Hao, J. Hazard. Mater. **262**, 782 (2013)
13. L. Zhang, J. Pierce, V.L. Leung, D. Wang, W.S. Epling, J. Phys. Chem. C **117**, 8282 (2013)
14. Y.Q. Zeng, Y.N. Wang, S.L. Zhang, Q. Zhong, W.L. Rong, X.H. Li, J. Colloid. Interfaces Sci. **524**, 8 (2018)
15. N.Y. Topsøe, Science **265**, 1217 (1994)
16. J. Yu, Z.C. Si, L. Chen, X.D. Wu, D. Weng, Appl. Catal. B: Environ. **163**, 223 (2015)
17. Y.C. You, C.N. Shi, H.Z. Chang, L. Guo, L.W. Xu, J.H. Li, J. Mol. Catal. **453**, 47 (2018)
18. W.Y. Yao, Y. Liu, X.Q. Wang, X.L. Weng, H.Q. Wang, Z.B. Wu, J. Phys. Chem. C **120**, 221 (2016)
19. T. Yi, Y.B. Zhang, J.W. Li, X.G. Yang, Chin. J. Catal. **37**, 300 (2016)
20. Q.L. Zhang, J.H. Zhang, Z.X. Song, P. Ning, H. Li, X. Liu, J. Ind. Eng. Chem. **34**, 165 (2016)
21. Y. Peng, K.Z. Li, J.H. Li, Appl. Catal. B: Environ. **140–141**, 483 (2013)
22. Z.C. Si, D. Weng, X.D. Wu, Z.R. Ma, J. Ma, R. Ran, Catal. Today **201**, 122 (2013)
23. Z.C. Si, D. Weng, X.D. Wu, R. Ran, Z.R. Ma, Catal. Commun. **17**, 146 (2012)
24. X.L. Weng, X.X. Dai, Q.S. Zeng, Y. Liu, Z.B. Wu, J. Colloid. Interf. Sci. **461**, 9 (2016)
25. Z.R. Ma, X.D. Wu, H. Härelind, D. Wen, B.D. Wang, Z.C. Si, J. Mol. Catal. A-Chem. **423**, 172 (2016)
26. Z.M. Liu, H. Su, J.H. Li, Y. Li, Catal. Commun. **65**, 51 (2015)
27. Z.X. Song, Q.L. Zhang, Y.X. Ma, Q.X. Liu, P. Ning, X. Liu, J. Wang, B. Zhao, J.H. Huang, Z.Z. Huang, J. Taiwan. Inst. Chem. E. **71**, 277 (2017)

28. Z.X. Song, L.W. Wang, Q.L. Zhang, P. Ning, J. Hu, T. Tang, X. Liu, B. Li, J. Taiwan. Inst. Chem. E **000**, 1 (2018)
29. Z.X. Song, Q.L. Zhang, P. Ning, J. Fan, Y.K. Duan, X. Liu, Z.Z. Huang, J. Taiwan. Inst. Chem. E. **65**, 149 (2016)
30. Q.L. Zhang, J. Fan, P. Ning, Z.X. Song, X. Liu, L.Y. Wang, J. Wang, H.M. Wang, K.X. Long, Appl. Surf. Sci. **435**, 1037 (2018)
31. J. Fan, P. Ning, Z.X. Song, X. Liu, L.Y. Wang, J. Wang, H.M. Wang, K.X. Long, Q.L. Zhang, Chem. Eng. J. **334**, 855 (2018)
32. J. Arfaoui, A. Ghorbel, C. Petitto, G. Delahay, Appl. Catal. B: Environ. **224**, 264 (2018)
33. C. Gannoun, R. Delaigle, D.P. Debecker, P. Eloy, A. Ghorbela, E.M. Gaigneaux, Appl. Catal. A-Gen. **447–448**, 1 (2012)
34. C. Gannoun, A. Turki, H. Kochkar, R. Delaigle, P. Eloy, A. Ghorbel, E.M. Gaigneaux, Appl. Catal. B: Environ. **147**, 58 (2014)
35. P.J. Gong, J.L. Xie, D. Fang, X.Q. Liu, F. He, F.X. Li, Chem. Eng. J. **356**(598), 598 (2019)
36. D. Wang, Y. Peng, Q.L. Yang, F.Y. Hu, J.H. Li, J. Crittenden, Catal. Today **332**, 42 (2019)
37. L. Wei, S.P. Cui, H.X. Guo, X.Y. Ma, J. Mol. Catal. A-Chem. **445**, 102 (2018)
38. L. Wei, S.P. Cui, H.X. Guo, L.J. Zhang, Comput. Mater. Sci. **144**, 216 (2018)
39. J.P. Wang, Z. Yan, L.L. Liu, Y. Chen, Z.T. Zhang, X.D. Wang, Appl. Surf. Sci. **313**, 660 (2014)
40. Q. Li, H.C. Gu, P. Li, Y.H. Zhou, Y. Liu, Z.N. Qi, Y. Xin, Z.L. Zhang, Chin. J. Catal. **35**, 1289 (2014)
41. S.X. Wang, R.T. Guo, W.G. Pan, Q.L. Chen, P. Sun, M.Y. Li, S.M. Liu, Catal. Commun. **89**, 143 (2017)
42. J.M.G. Amores, V.S. Escribano, G. Ramis, G. Busca, Appl. Catal. B: Environ. **13**, 45 (1997)
43. S.C. Xiong, Y. Liao, X. Xiao, H. Dang, S.J. Yang, J. Phys. Chem. C **119**, 4180 (2015)
44. D. Wang, L. Zhang, K. Kamasamudram, W.S. Epling, ACS Catal. **3**, 871 (2013)
45. C. Gao, J.W. Shi, Z.Y. Fan, B.R. Wang, Y. Wang, C. He, X.B. Wang, J. Li, C.M. Niu, Appl. Catal. A-Gen. **564**, 102 (2018)
46. G.Y. Zhou, B.C. Zhong, W.H. Wang, X.J. Guan, B.C. Huang, D.Q. Ye, H.J. Wu, Catal. Today **175**, 157 (2011)
47. S.W. Liu, R.T. Guo, X. Sun, J. Liu, W.G. Pan, Z.L. Xin, X. Shi, Z.Y. Wang, X.Y. Liu, H. Qin, J. Energy Inst. **92**, 1610 (2018)
48. X.J. Yao, Z. Wang, S.H. Yu, F.M. Yang, L. Dong, Appl. Catal. A-Gen. **542**, 282 (2017)
49. F.Y. Gao, X.L. Tang, H.H. Yi, S.Z. Zhao, J.G. Wang, T. Gu, Appl. Surf. Sci. **466**, 411 (2019)
50. D. Wang, Y. Peng, S.C. Xiong, B. Li, L.N. Gan, C.M. Lu, J.J. Chen, Y.L. Ma, J.H. Li, Appl. Catal. B **221**, 556 (2018)
51. S.H. Zhan, H. Zhang, Y. Zhang, Q. Shi, Y. Li, X.J. Li, Appl. Catal. B **203**, 199 (2017)
52. C.L. Yu, B.C. Huang, L.F. Dong, F. Chen, X.Q. Liu, Catal. Today **281**, 610 (2017)
53. L. Chen, J.H. Li, M.F. Ge, Environ. Sci. Technol. **44**, 9590 (2010)
54. M.Y. Li, R.T. Guo, C.X. Hu, P. Sun, W.G. Pan, S.M. Liu, X. Sun, S.W. Liuand, J. Liu, Appl. Surf. Sci. **436**, 814 (2018)
55. S.J. Yang, Y. Liao, S.C. Xiong, F.H. Qi, H. Dang, X. Xiao, J.H. Li, J. Phys. Chem. C **118**, 21500 (2014)
56. N.Z. Yang, R.T. Guo, W.G. Pan, Q.L. Chen, Q.S. Wang, C.Z. Lu, S.X. Wang, Appl. Surf. Sci. **378**, 513 (2016)